2D WATER-WAVE INTERACTION WITH PERMEABLE AND IMPERMEABLE SLOPES: DIMENSIONAL ANALYSIS AND EXPERIMENTAL OVERVIEW

Pilar Díaz-Carrasco[1*], Mª Victoria Moragues[1], María Clavero[1], Miguel Á. Losada[1]

[1]Andalusian Institute for Earth System Research, University of Granada, Avda. del Mediterráneo, s/n, 18006, Granada, Spain

Abstract

The main objective of this research is to characterize and quantify the prevalent physical processes in the energy transformation of a regular wave train when it interacts with permeable and impermeable breakwaters. Two sources of experimental data are considered: (a) numerical experiments on an undefined impermeable rigid slope, using the numerical model (IH-2VOF), and (b) physical experiments on a non-overtoppable permeable breakwater with a cube armor layer and a porous core of finite width in a 2D wave flume. A revised dimensional analysis reveals that the relative water depth, h/L, and the incident wave steepness, H/L, at the toe of permeable and impermeable breakwaters are the key factors to define and optimize the experimental space (H_I/L, h/L). Moreover, the product of $(h/L)(H_I/L)$ can be applied to identify the type of wave breaking and the domains of wave energy transformation, and to quantify the reflected and transmitted energy coefficients and the dissipation rate (K_R^2, K_T^2, D^*). Fitting an experimental curve (i.e. a sigmoid function) to the impermeable data, the slope is a plotting parameter. The same conclusion is obtained for a permeable breakwater; in addition the wave energy coefficients depend on the relative breakwater width B^*/L, and the relative core grain size and $D_{50,p}/L$, and armor unit diameter, D_a/L. Because the range of the design factors spans several orders of magnitude, a log-transformation provides a well behaved experimental space [ln(h/L), ln(H/L)] which is likely of benefit to verify the wave breaker type and the related dissipation-reflection-transmission on slopes. Finally, this study shows that there is not a biunivocal relationship between the Iribarren number, I_r, and the type of breaker, the reflection and transmission coefficients and the bulk dissipation. Therefore, Iribarren's number is not a sufficient similarity parameter for the analysis of wave breaking, and related flow characteristics on slopes.

Keywords: *Breakwater, Iribarren number, experimental tests, bulk wave dissipation, wave reflection, wave transmission*

*Corresponding author

E-mail address: pidiazc@ugr.es (P. Díaz-Carrasco)

1. Introduction

The main function of breakwaters is to protect harbors and coastal structures from wave action. They are an important type of coastal and port infrastructure because of their functionality as well as their cost, design complexity, and environmental and socioeconomic impacts. The conception, design, and verification of a breakwater mainly depends on the slope of the sea bottom, water depth at the breakwater toe, h, and the characteristic values of incident waves H, T, θ (height, period, and incidence angle). They also depend on the available materials, construction and repair techniques, and the consequences that ensue when and if objectives are not attained. The performance of the breakwater against wind waves is mainly determined by the slope on both sides of the breakwater, shape and weight of the unit pieces, number of armor layers, thickness and emplacement of the main layer/secondary layers and the width, crest elevation, and size of the core materials (ROM 0.0, 2001; ROM 1.1, 2019).

Battjes (1974) proposed using the Iribarren number (Iribarren and Nogales, 1949), $I_r = \tan(\alpha)/\sqrt{H/L}$, as the dynamic similarity parameter to analyze wave train behavior on an indefinite impermeable flat slope, slope angle α, where L is the characteristic wavelength. He also conjectured that the value of I_r identified breaker type as spilling, plunging, collapsing, or surging (Iversen, 1952; Galvin, 1968). Furthermore, he anticipated its capacity to determine the phase difference and wavebreaking index, wave run-up and run-down, mean level, and the reflection and dissipation (absorption) of the waves on the breakwater slope.

In the field of harbor and maritime structures (and also beach morphodynamics), the seminal work of Battjes (1974) led to research whose objective was to determine the transformation of incident energy when waves interacted with the breakwater by means of the reflected energy coefficient, K_R^2, transmitted energy coefficient, K_T^2, and the bulk dissipation rate, D^*. Still another objective was to develop formulas for wave run-up, run-down, overtopping and stability of the main armor layer in the domain of interest, $I_r > 1.5$, as reflected in the following references, among others: Brunn and Günbak (1976); Losada and Giménez-Curto (1981); Seelig and Ahrens (1981); Allsop and Hiettrarchi (1989); Martin et al. (1999); Zanuttigh and Van der Meer (2008); Burcharth et al. (2010); Van der Meer (2011); Gómez-Martín and Medina (2014); Vílchez et al. (2016a).

These studies show that in the domain, $I_r > 1.5$, the Iribarren number reveals the general tendency of coefficients [K_R^2, K_T^2]. However, the values tend to scatter as the value of I_r increases, depending on the slope angle. Energy transmission at a non-overtopped breakwater is usually small, $K_T^2 < 0.15$, but this information is necessary in order to evaluate the bulk dissipation at the structure. Nonetheless, there are relatively few articles on the calculation of wave dissipation and is still an open quention. Such studies include the following, among others: Seelig and Ahrens (1981); Kobayashi and Wurjanto (1992); Pérez-Romero et al. (2009); Van Gent et al. (2013); and Vílchez et al. (2016b).

Forty years after Battjes (1974), physical experiments on breakwaters are still based on the working hypothesis that the Iribarren number is a dynamic similarity parameter between model and prototype, and that, generally speaking, the Iribarren number is the main variable in formulas that determine the wave energy transformation coefficients [K_R^2, K_T^2, D^*] for a breakwater and related hydrodynamic performance.

Over the last thirty years, research studies have questioned the dependence of $K_R^2 = f(I_r)$. Hughes and Fowler (1995), and Sutherland and O'Donoghue (1998) applied the parameter x_m/L (where $x_m = h/tg(\alpha)$) to also quantify the phase of the reflected wave train. Davidson et al. (1996) defined a reflection number that includes I_r and the characteristic diameter of the armor layer. Van der Meer (1988, 1992) incorporated a permeability parameter and fit the exponents of I_r by means of a multiple regression analysis. Benedicto (2004) analyzed wave reflection, depending on h/L and grain size. Finally, Vílchez et al. (2016a) modifies the Iribarren number to incorporate, grain diameter, and the width and depth of the breakwater core in a single parameter.

The main objectives of this research were the following: (1) to collate the dependence of wave energy transformation processes (reflection, transmission, and bulk dissipation rate) with Iribarren number; (2) to apply dimensional analysis to the design of experiments for both a permeable and impermeable slope; and (3) to analyze the variability of the results and identify those characterized by the hydrodynamic performance of the breakwater. This study involved numerical experiments using an undefined, impermeable, rigid slope and the application of the IH-2VOF model (Lara et al., 2008). These were combined with laboratory experiments in the 2D flume of a non-overtoppable mound breakwater with a cube layer and porous core of finite width. Linear wave theory was applied to separate the incident, reflected, and transmitted time series of the data records of the vertical displacement of the free surface at different points in the experimental setup. The wave energy conservation equation was applied to obtain the bulk dissipation rate on the breakwater.

The rest of this paper is organized as follows. Section 2 describes the theoretical background to understand the main aspects of the physical processes that intervene in the water-wave interaction with the breakwater. Section 3 presents the experimental design, analysis and setups (numerical and physical) performed in this study and presented in terms of I_r. Section 4 presents the numerical and physical results obtained. The results are initially represented, depending on the Iribarren number, after which they are displayed, depending on the dimensionless quantities obtained when the dimensional analysis was applied. Section 5 discusses the results, evaluates their validity in reference to the hypothesis and the experimental desviation obtained. Section 6 presents the conclusions derived from this research. Finally, the revised dimensional analysis of this study is outlined in Appendix A.

2. Background

The dissipation of a wave train on a breakwater slope is mainly caused by the generation, transport, and dissipation of turbulence during the following processes: (i) wave evolution and eventually wavebreaking on the free surface of the slope; (ii) interaction (circulation and friction) with the main armor layer; (iii) wave propagation through the secondary layers and porous core; and (iv) wave transmission leewards of the structure.

Reflection-dissipation-transmission in a porous medium

The theoretical formulation for the propagation of a regular or irregular wave train through a porous medium has been widely studied (Sollit and Cross, 1972; Dalrymple et al., 1991). Numerical and physical experiments have also been performed to address this topic (Pérez-Romero et al., 2009; Vílchez et al., 2016b). The Forchheimer equation is able to provide a reasonably accurate representation of the bulk resistance over the porous medium with coefficients that depend on the Reynolds and Keulegan-Carpenter numbers (Re_p, KC_p) (Van Gent, 1995; Pérez-Romero et al., 2009; Jensen et al., 2014a, b).

In the last 20 years, there have been various studies on numerical predictions of wavebreaking on a smooth impermeable slope by means of different techniques (Christensen and Deigaard, 2001; Lara et al., 2006; Zhang and Liu, 2006; Madsen and Furham, 2008; Gíslason et al., 2009; Lakehal and Liovic, 2011). These results provide a detailed picture of the spatio-temporal evolution of the wave on the slope and help to clarify the origin of the variability and experimental scattering of the results obtained in physical experiments. In the interval, $1.5 < I_r < 3.5$, four breaker types can be identified: weak plunging and strong plunging (Lakehal and Liovic, 2011) and weak bore and strong bore (Zhang and Liu, 2008).

Furthermore, reflection and dissipation during shoaling and the eventual breaking of the wave on a slope with a permeable core do not have a theoretical model equivalent to the Forchheimer equation. Accordingly, most studies are based on numerical and physical experiments (Kobayashi and Wurjanto, 1992; Lara et al., 2008; Zanuttigh and Van der Meer, 2008; Ruju et al., 2014; Jensen et al., 2014a, b; Vanneste and Troch, 2015; Vílchez et al., 2016a, b; Clavero et al., 2018). The following results are relevant to this study:

1. The presence of a porous core is relevant to the hydrodynamic performance of the breakwater because it determines the phase lag between the incident and reflected wave trains and its impact on breaker type.
2. The dimensions of the main armor layer and its unit pieces significantly influence the values of reflected energy dissipation as well as the dissipation rate.
3. Design formulas for mound breakwaters are usually based on experimental data, whose scattering is usually maximum in the interval of I_r corresponding to the critical design conditions. These formulas are generally applied to calculate the transformation of incident energy, run-up and run-down, and when applicable, the overtopping volume and the stability of the breakwater units.

Model of hydrodynamic behavior

When a wave train interacts with a breakwater, its behavior depends on the transformation process, which dominates the spatio-temporal evolution of the wave train that propagates onto the slope and porous core. In the case of spilling breakers, the process is gradually dissipative and depends on the characteristics of the wave train at undefined depths, $(H/L)_0$ and its shoaling at the slope. The shoaling depends on x_m/L, where $x_m = h/tg(\alpha)$ should be very small. In other words, reflection should be negligible on the slope as well as in the porous core. Spilling breakers and weak plunging breakers satisfy these conditions. If the wave train surges on the slope and propagates through the porous nucleus, the transformation process is essentially reflective. This process is described by the slope angle α, relative depth h/L, width B^*/L and the relative diameters of the core, $D_{50,p}/L$. Dissipation, which is small, occurs on the main armor layer (or the rough granular bed) as well as inside the breakwater core. The phase depends on x_m/L and $D_{50,p}/L$, B^*/L, and determines the location of the nodes and anti-nodes of the wave.

These modes of wave-train transformation and their related breaker types are the following: (i) dissipative mode typical of spilling breakers and weak plunging breakers; (ii) reflective mode for surging "breakers"; and (iii) transitional modes. In this work, three types of wave-train transformation and their corresponding breaker type, namely, strong plunging breakers, strong bores, and weak bores are identified as transitional modes. If wave reflection is not negligible (on the slope and in the core), the phase lag between the incident and reflected wave trains affects the location of the breaker point and determines the breaker type. If the amount of reflected energy and the dissipation rate are similar, the most probable breaker types are: strong plunging, strong bores or weak bores, depending on the place where most of the energy is reflected, namely, the breakwater slope or core, (Losada et al. 2019).

Turbulence processes in these three breaker types have multiple scales. Locally, turbulence generation and turbulence dissipation are not in equilibrium, and so the spatio-temporal evolution of the wave train has an intrinsic variability associated with the transport of the turbulent kinetic energy (TKE). The transition from one breaker type to another can be sudden or gradual, and the three can occur with different value pairs of H_I/h and h/L, depending on the slope angle, α, and the characteristics of the main armor layer and the permeable core.

The experimental design and the dimensional analysis carried out in this work are based on the background described in this section.

3. Experimental design and setup

This research study is based on the following: (a) numerical experiments, using the IH-2VOF model (Lara et al., 2008), on a mound breakwater with an undefined, impermeable, rigid slope; (b) physical experiments using a wave flume, on a mound breakwater with a non-overtoppable permeable constant slope, a cube armor layer and a porous core of constant finite width, B^*, and grain size, $D_{50,p}$. The flume bottom is horizontal and the water depth in the wave generation zone and in the flume up to the toe of the slope is constant, h.

3.1 Physical tests

The experimental tests were performed in the wave-current flume (23x0.65x1m) of the Andalusian Inter-University Institute for Earth System Research (IISTA) at the University of Granada. Figure 1 shows a diagram of the physical model tested, namely, a permeable mound breakwater with a main armor layer consisting of two layers of cubes with a porous core. See Table 1 for more details regarding the geometrical configuration of the model. The water depth was kept constant and equal to h=0.4 m.

Tests were performed in the wave flume with a VTI controller. The AwaSys software package was used to generate waves with the simultaneously active absorption of reflected waves. Regular waves were simulated and defined by a wave height, H_{target}, and wave period T_{target}. Wavebreaking was only caused by wave-breakwater interaction, and the experiments were under non-overtopping and non-damage conditions. Table 2 shows the target wave parameters run in each configuration.

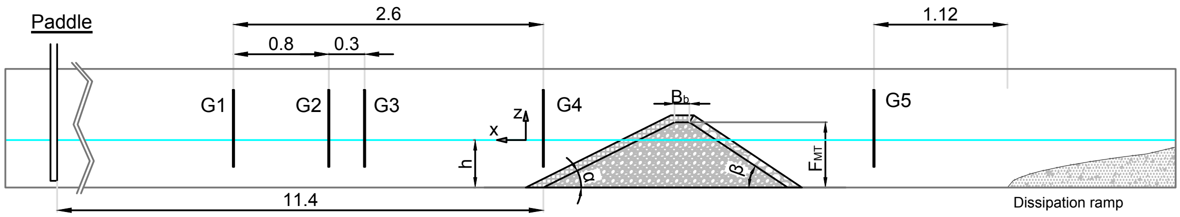

Figure 1. Diagram of the wave flume and location of wave gauges (dimensions in meters).

.

Breakwater geometry					Porous medium				
Armor unit: cubes (m)	B_b (m)	ρ_s (tn/m^3)	$\cot(\alpha)$	$\cot(\beta)$	F_{MT} (m)	$D_{50,p}$ (m)	A_{eq} (m^2)	ρ_s (tn/m^3)	n_p
l =0.033 D_{eq} =D_a = 0.0409	$3D_a$	2.18	2	1.5	0.55	0.012	0.2125	2.84	0.39

Table 1. Geometric parameters of the physical model: B_b is the width of the top of the breakwater; F_{MT} is the porous medium height; D_{eq} is the equivalent diameter of the main armor layer (the characteristic armor diameter D_a), where the cube volume is equated to the volume of a sphere; A_{eq} is the area of the porous core per section unit below mean sea level (Vílchez et al., 2016a); $\cot(\alpha)$ and $\cot(\beta)$ are the leeward and landward slopes of the breakwater, respectively; ρ_s is the density of the unit pieces; and np is the porosity of the core, according to CIRIA/CUR/CETMEF (2007).

Four Iribarren numbers, $I_{r\ target}$ were tested (see Table 2) in the domain of interest (I_r >1.5), following two ways of wave generation sequence: (1) $I_{r\ target,H}$, the wave height remained constant, whereas the wave period ($T_{target,\mathrm{H}}$) varied; (2) $I_{r\ target,T}$, the wave period remained constant, whereas the wave height ($H_{target,\mathrm{T}}$) varied. Each test was repeated three times and 100 waves were simulated in each test.

$I_{r,target}$		2.30	3.00	3.70	5.00
$I_{r\ target,H}$	H_{target} (m)	[0.07 - 0.12]	[0.05 - 0.12]	[0.04 - 0.10]	[0.02 - 0.80]
	$T_{target,\mathrm{H}}$ (s)	[1.00 – 1.47]	[1.14 – 2.30]	[1.31 – 2.86]	[1.23 – 4.10]
$I_{r\ target,T}$	T_{target} (s)	[1.05 – 1.50]	[1.25 – 2.50]	[1.25 - 3.00]	[1.25 - 3.00]
	$H_{target,\mathrm{T}}$ (m)	[0.075 – 0.124]	[0.057 – 0.133]	[0.038 – 0.105]	[0.021 – 0.058]

Table 2. Wave conditions tested in the laboratory (target values for the two ways of wave generation sequence).

3.2 Numerical tests

The IH-2VOF numerical model (Lara et al., 2008) was used to study a breakwater with a non-overtoppable, impermeable, smooth slope with three leeward slope angles ($\cot\alpha = 2, 3$ and 10). For more details of the configuration of the model, see Table 3.

The wave flume of the IISTA was reproduced in the numerical model with a 2D domain. The numerical set-up was the same used and calibrated in Vílchez et al. (2016b), formed by a uniform grid on the *y*-axis with a grid cell size of 0.5 cm, and horizontally (on the *x*-axis) grid with three regions: (i) a center region, 5 m long, containing the breakwater section with the finest resolution and a cell size of 1 cm; two regions (ii) at the beginning and (iii) at the rear of the numerical wave flow with a cell size of 2 cm. A mesh sensitivity analysis was performed to assess the computational costs and the accuracy of the results. The total number of cells in the numerical domain was 1304 × 162. Active wave absorption was used at the generation boundary, and the dissipative ramp at the end of the flume was reproduced with a porous medium.

Breakwater geometry					Wave conditions		
Armor +core	B_b	$\cot(\alpha)$	$\cot(\beta)$	F_{MT}	h	T_{target}	$I_{r,target}$
Impermeable	0.5 m	2	-	0.75 m	0.4 m	[1-2.2] s	[2.3, 3.0, 3.5, 4, 5]
	0.5 m	3	-	0.65 m	0.35 m	[1-2.2] s	[1.5, 1.8, 2.3, 3.0, 3.5, 4.0, 5.0]
	0.5 m	10	-	0.65 m	0.35 m	[1-2.2] s	[0.5, 1.5, 1.8, 2.3, 3.0, 3.5, 4.0]

Table 3. Wave parameters and geometric configuration of the breakwater in the numerical model.

Regular waves were simulated by setting T and varying H to cover the Iribarren domain (I_r >1.5). Two water depths were tested: (1) h=0.35 m, the same as in Moraes (1970); and (2) h=0.4 m, the same as in the physical model (see Table 3). To complete the study of breakwater performance, some cases were simulated in domain I_r < 1.5 with a slope of 1:10.

3.3 Time series analysis and evaluation of the bulk dissipation

The incident and reflected wave trains were separated by applying Baquerizo (1995), (based on Mansard and Funke´s (1987) three-gauge method), providing the magnitude and phase of the reflected wave train. The reflected and transmitted wave energy, E_R, E_T, and their respective reflection (K_R^2 and phase φ_R) and transmission coefficients (K_T^2), that is, the dependent quantities of the dimensional analalysis (Appendix A), were obtained by applying power spectral analysis. K_R^2 and φ_R were calculated with the data measured by gauges G1, G2 and G3 (see Fig. 1). The transmission coefficient (K_T^2) was computed with the data measured with gauge G5. Gauge G4, located at the toe of the structure (x = 0), provided the total wave height at the toe of the breakwater (due to the interaction of the incident and reflected wave trains). For the numerical setup, wave gauges were placed in the numerical model at the same location as the ones used in the physical experiments.

The dependent quantities satisfy the energy conservation equation in a finite control volume (CV) with a unit width and constant depth that includes the breakwater, (positive inflow, negative outflow and dissipation flow)

$$F_I - F_R - F_T - D'^* = 0 \tag{1}$$

Where $F_i = C_{g,i}E_i = (1/8)\,\rho g C_{g,i} H_i^2$; i= I, R, T represents the mean energy flow of the incident, reflected, and transmitted wave trains, respectively; ρ is the water density; and $C_{g,i}$ is the group celerity of the energy propagation. D'^* is the mean bulk dissipation, due to wavebreaking on the slope, and where applicable, wave interaction with the main armor layer and propagation through the porous core.

4. Results

This section presents the results of the wave transformation coefficients [K_R^2, K_T^2, D^*] for the two configurations: (impermeable and permeable) non-overtoppable mound breakwater.

4.1 Iribarren number as a breakwater similarity parameter

4.1.1 Impermeable and non-overtoppable slope

Figure 2 represents the numerical results of K_R^2 and D^* against the Iribarren number, nine target values (Fig. 2 a1,b1), and three slopes, [1/10 ≤$\tan(\alpha)$≤ 1/2] (Fig. 2 a2, b2). The behavior of the data is similar to Battjes (1974) (his Figure 2 with data from Moraes, 1970). The left panels of Figure 2 provide the values of $I_{r,target}$ for each experiment, which were generated by fixing T and varying H. The x-axis shows the experimental Iribarren number, $I_{r,I}$, calculated with incident wave height H_I. The bulk dissipation, D^*, against I_r mimics the reflected energy coefficient, K_R^2. Moreover, the blue bands indicate the confidence interval (5%-95%) of the values thus calculated for each chosen $I_{r,target}$.

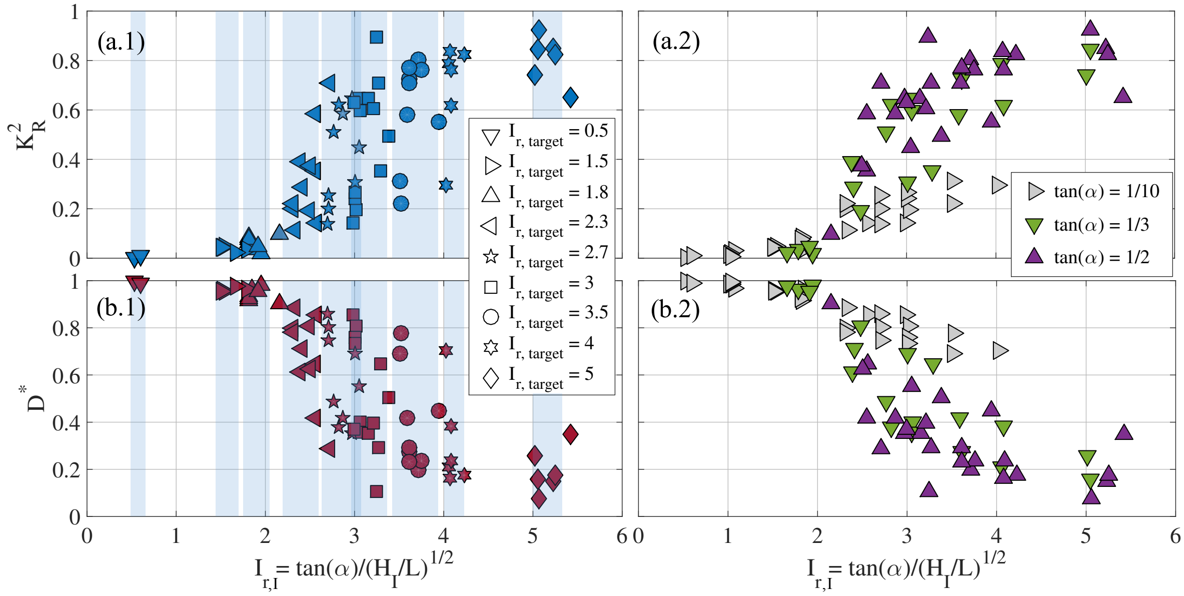

Figure 2. Impermeable and non-overtoppable slope. Experimental numerical results (IH-2VOF) of the transformation of incident waves against the experimental Iribarren number ($I_{r,I}$): (a) modulus of the reflected energy coefficient (K_R^2) y (b) simulated bulk wave dissipation, numerically simulated according to, (a1, b1) $I_{r,target}$; (a2, b2) slope angle. The blue bands represent the confidence intervals of 5%-95% for each $I_{r,I}$, target value.

For the three slopes, K_R^2 disposition depends on the slope angle. Scattering decreases as the slope decreases, and increases when $I_{r,I}$ is in interval [$2.2 \leq I_{r,I} \leq 4.2$]. As can be observed, the variability of each slope angle in each interval (blue band) is significant with slight changes in the value of $I_{r,I}$. This variation mainly stems from small variations in the incident wave height H_I. Nevertheless, "local" scattering (for $I_{r,I}$ intervals) does not decrease when the set of wave trains corresponding to a value of $I_{r,target}$ was repeated.

Figure 3 represents K_R^2 and D^* against the incident wave steepness, H_I/L. It is observed that the numerical data are better ordered and the dispersion is slightly less compared to Iribarren number. However, the variability is still significant, in particular for higher values of the wave reflection coefficient. For example, for a given value of $H_I/L = 2.5 \cdot 10^{-2}$, the reflected energy coefficients are in interval $0.42 < K_R^2 < 0.9$ for the slope 1:2.

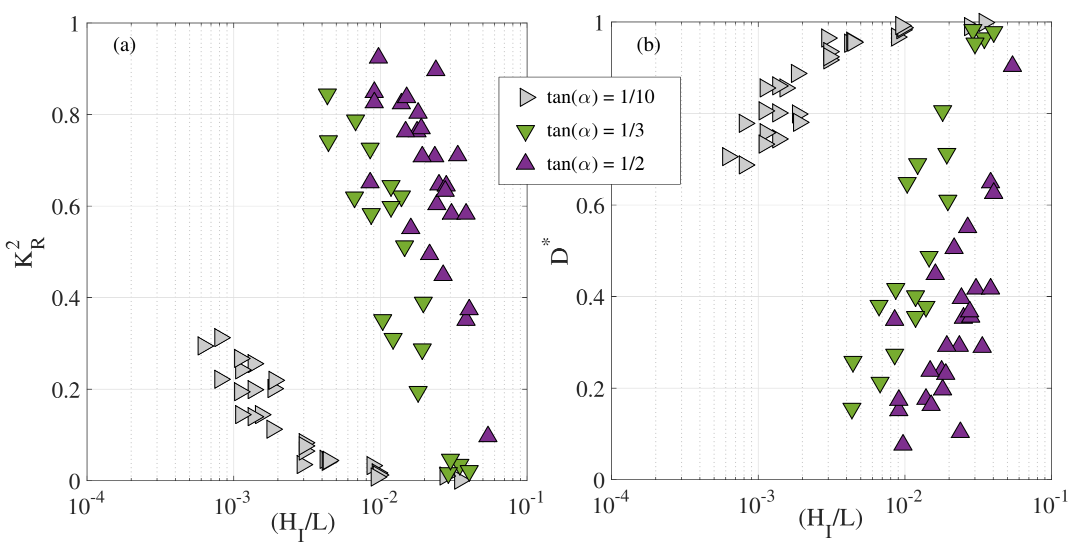

Figure 3. Impermeable and non-overtoppable slope. Experimental numerical results (IH-2VOF) of the transformation of incident waves against the incident wave steepness (H_I/L): (a) modulus of the reflected energy coefficient (K_R^2) y (b) simulated bulk wave dissipation, numerically simulated according to the slope angle.

4.1.2 Permeable with a main armor layer and non-overtoppable slope

Figure 4 presents the physical experimental results of K_R^2, K_T^2 and D^*, against $I_{r,I}$ (inside the domain $I_r \geq 1.5$), obtained from the permeable slope of 1:2. $I_{r,target}$ values were set either by maintaining H constant and varying T, or by maintaining T constant and varying H, (Fig. 4a). The calculation of the real value $I_{r,I}$ is based on the incident wave height H_I, which was obtained by separating the incident and reflected wave trains (Section 3.3). These experiments also determined K_T^2, (Fig. 4c). The transmitted energy is one order of magnitude lower than the reflected energy. The energy conservation equation is applied to obtain the bulk dissipation D^* (Fig. 4b).

Experimental scattering increases with $I_{r,I}$ in the interval $[2.2 \leq I_{r,I} \leq 4.2]$. The experimental scatter of each interval (blue band) is significant with slight changes in the value of $I_{r,I}$. This variation is mainly due to small variations in the incident wave height H_I and interaction with the reflected wave train, (modulus and phase). The same value of the Iribarren number can have different energy transformation modes and, consequently, different potential breaker types. Local scattering (for intervals de $I_{r,I}$) does not decrease when the experiment for a given value of $I_{r,target}$ is repeated.

Present results, for permeable and impermeable slopes as well, show that the transformation of incident energy on an undefined slope roughly depends on I_r. Nevertheless, they also raise questions regarding the application of the Iribarren number as a relevant parameter, to quantify the energy transformation modes and, consequently, the potential breaker types.

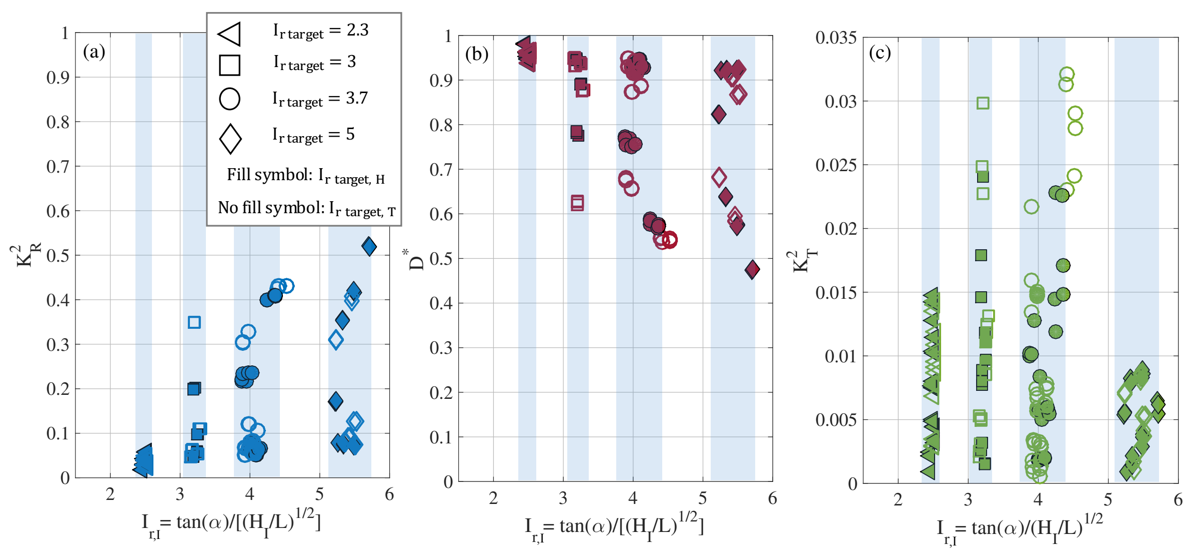

Figure 4. Permeable with a main armor layer and non-overtoppable slope. Results of the physical experiments (IISTA-UGR) on incident wave transformation against the experimental Iribarren number l($I_{r,I}$): (a) modulus of the reflected energy coefficient (K_R^2), (b) bulk wave dissipation y (c) modulus of the transmitted energy coefficient (K_T^2) according to the $I_{r,target}$. The blue band represents the confidence level (5%-95%) for each $I_{r,I}$, target value.

4.2 An alternative breakwater similarity parameter: χ =(h/L)(HI/L)

This section presents the same physical and numerical data of Figures 2, 3 and 4 against the non-dimensional parameter $(h/L)(H_I/L)$, derived from the reformulation of the dimensional analysis (Appendix A).

4.2.1 Impermeable and non-overtoppable slope

Figure 5 represents K_R^2, against the product of relative wave steepness, H_I/L, and relative depth, h/L, As in Figures 2 and 3, the slope is also identified. The *x*-axis is represented on a semi-logarithmic scale to facilitate the visualization of the data. The values are separated, depending on the slope. For a given value of $(h/L)(H_I/L)$ the experimental scattering becomes greater as the slope angle increases.

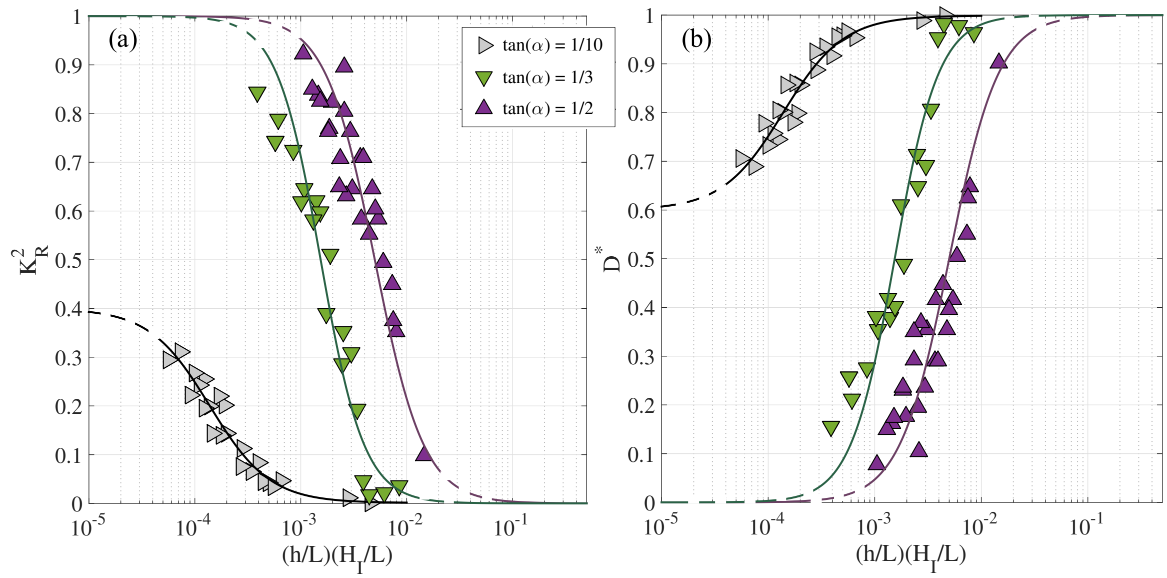

Figure 5. Impermeable and non-overtoppable slope. Experimental numerical results (IH-2VOF) of the incident wave energy transformation against (h/L)(H_I/L): (a) modulus of the reflected energy coefficient (K_R^2 -Eq. 3- Appendix A); (b) bulk wave dissipation (D^*-Eq. 4- Appendix A) depending on the slope angle. The solid lines represent the sigmoid curves (Eq. 2) fit to each slope (see Table 4 for the fit parameters) and the dash lines represent the choosen limit values for fitting the curves.

4.2.2 Permeable with a main armor layer and non-overtoppable slope

Figures 6a, 6b, and 6c represent the values of K_R^2, D^* and K_T^2, respectively, against the product of the relative wave steepness and the relative width on the *x*-axis at a semi-logarithmic scale. For purposes of comparison, the figures also represent the experimental data numerically obtained for the same 1:2 slope. For the permeable slope, the vertical dispersion of K_R^2 is greater in the interval $5 \cdot 10^{-4} < (h/L)(H_I/L) < 3 \cdot 10^{-3}$, which differs from the interval of greatest dispersion for the impermeable slope. The horizontal dispersion (same value of the energy coefficient) is possibly due to the different mode of energy transformation and the potential associated breaker types. Figure 7 shows the same information as Figure 6, but this time, the values of the relative characteristic width of the breakwater are identified.

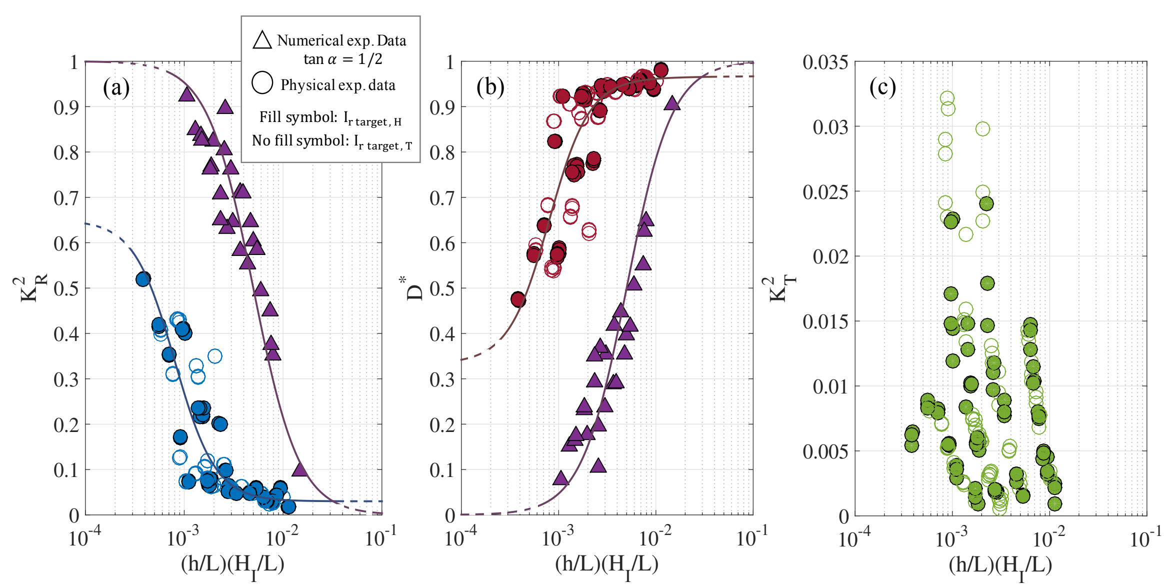

Figure 6. Physical results (circles - IISTA-UGR) and numerical results of the slope 1:2 (triangles - IH-2VOF) for the incident wave transformation against (h/L)(H_I/L): (a) modulus of the reflected energy coefficient (K_R^2 -Eq. 5- Appendix A), (b) bulk wave dissipation (D^*-Eq. 7- Appendix A) and (c) modulus of the transmitted energy coefficient (K_T^2 -Eq. 6- Appendix A). The solid lines represent the sigmoid curves (Eq. 2) with the best fit to the experimental data K_T^2 and D^*. The fit parameters are shown in Table 4 and the dash lines represent the choosen limit values for fitting the curves.

In all cases, the energy transmitted is very small, and thus the increase in K_R^2 is mostly compensated by the decrease in dissipated energy D^* (Figs. 6 and 7). The vertical scale of the figure highlights the fact that the data of K_T^2 cluster, based on the relative width (or relative diameter) of the breakwater. Its value increases when there is a decrease in B^*/L, (or $D_{50,p}/L$) as well as its growth rate. This behavior is also observed in K_R^2 (and consequently in D^*), especially when the reflected energy is very small and energy dissipation is the dominant process (Figs. 7b and 7b). Given that $D_{50,p}$ and B^* are constant and become dimensionless with the wavelength, the experimental scatter of K_R^2, D^* and K_T^2, for $D_{50,p}/L$ L is equivalent as for B^*/L in Figure 6.

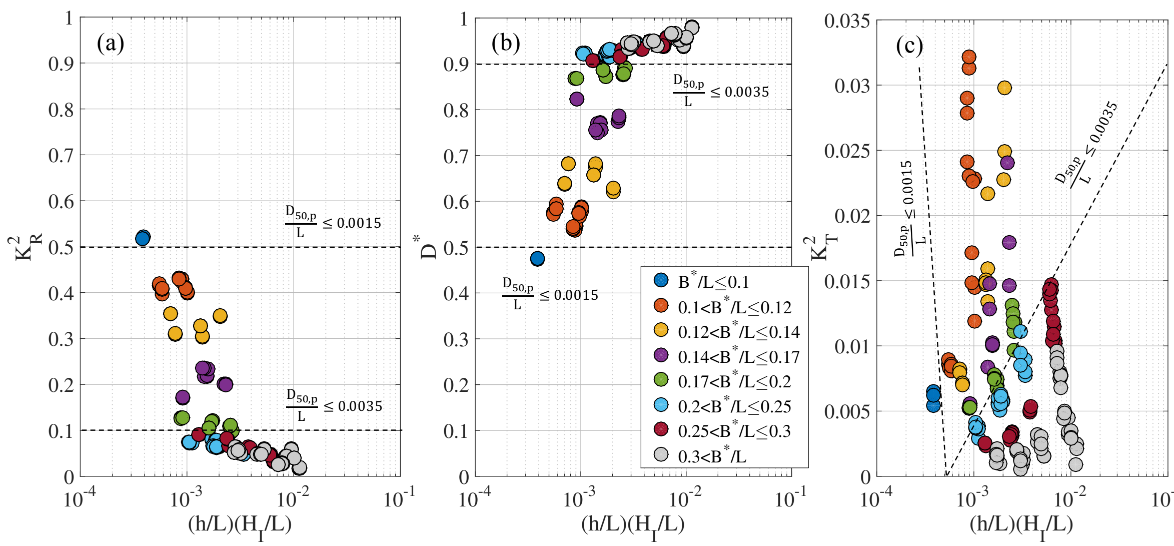

Figure 7. Physical results (IISTA-UGR) of the incident wave transformation against (h/L)(H_I/L): (a) modulus of the reflected energy coefficient (K_R^2 -Eq. 5- Appendix A), (b) bulk wave dissipation (D^*-Eq. 7- Appendix A) and (c) modulus of the transmitted energy coefficient (K_T^2 -Eq. 6- Appendix A) according to intervals of values of B^*/L. The dotted line marks the limit of $D_{50,p}$/L where $K_R^2 > 0.5$ y D^*>0.9.

5. Discussion

This section discusses the aspects of the function fitted to the data and the experimental deviation technique that could have influenced or conditioned the results presented in Section 3.

5.1 Sigmoid curves and domains of wave energy transformation

The sigmoid curve is chosen to fit the experimental results according to $\chi = (h/L)(H_I/L)$, since it is successfully to describe various physical phenomena in fluid mechanics, heat transfer and chemical engineering (Churchill and Usagi, 1972; Sivanesapillai et al., 2014; Vílchez et al., 2016a),

$$X(\chi) = (X_1 - X_0)\left[1 + \left(\frac{\chi}{a_\chi}\right)^{\gamma_\chi}\right]^{-1} + X_0; \quad \chi > 0 \tag{2}$$

where $X(\chi) = [K_R^2, K_T^2, D^*]$ is the physical entity and X_0, X_1 are the choosen limit values of $X(\chi)$ for fitting the curves for a small and large values of the independent dimensionless variable χ=$(h/L)(H_I/L)$. It describes a uniform transition between the limit values with a blending coefficient, γ_χ, and a parameter of the process inherent to the sigmoid shape, a_χ.

Table 4 gathers the parameters of the sigmoid functions fitted to the impermeable and permeable experimental results (Section 4). The sigmoid parameters (Table 4) show that the sigmoid shape, a_χ, is specific for each slope angle tested.

Mound breakwater	Sigmoid function	Fit parameters			
	$K_R^2 = (K_{R1}^2 - K_{R0}^2)\left[1+\left(\frac{(h/L)(H_I/L)}{a_\chi}\right)^{\gamma_\chi}\right]^{-1} + K_{R0}^2$	K_{R0}^2	K_{R1}^2	a_χ	γ_χ
Impermeable	$\tan\alpha = 1/2$	0	1	0.005	1.8
	$\tan\alpha = 1/3$	0	1	0.002	2.1
	$\tan\alpha = 1/10$	0.001	0.4	0.00012	1.5
Permeable	$\tan\alpha = 1/2$	0.03	0.65	0.0008	2.1

Table 4. Parameters for the sigmoid curves (Eq.2) fitted to the experimental data K_R^2 and D^*. Since K_T^2 values are an order of magnitude lower than K_R^2 values, the sigmoid curve are not fitted.

For practical engineering purposes, it is advisable to identify at least three domains of incident wave behavior according to $(h/L)(H_I/L)$ values and the shape of the sigmoid curve. Hence, the threshold values that limit the domains of energy transformation are specific for each slope of the breakwater tested.

For an impermeable breakwater with slope 1:2,

- Reflective domain, $\{K_R^2 \geq 0.9\}$: $(h/L)(H_I/L) < 1.1 \cdot 10^{-3}$;
- Dissipative domain, $\{D^* \geq 0.9\}$: $(h/L)(H_I/L) > 1.1 \cdot 10^{-2}$;
- Transitional domain, $\{0.1 < K_R^2 < 0.9\}$: $1.1 \cdot 10^{-3} < (h/L)(H_I/L) < 1.1 \cdot 10^{-2}$

For a permeable breakwater with a constant slope 1:2 and a core with a B^*/L and $D_{50,p}/L$,

- Reflective domain, $\{K_R^2 \geq 0.5\}$: $(h/L)(H_I/L) < 4.5 \cdot 10^{-4}$, with $[D_{50,p}/L \leq 0.0015, B^*/L \leq 0.10]$
- Dissipative domain, $\{D^* \geq 0.9\}$: $(h/L)(H_I/L) > 2 \cdot 10^{-3}$, with $[D_{50,p}/L > 0.0035; B^*/L > 0.20]$
- Transitional domain, $\{0.1 < K_R^2 < 0.5, 0.5 < D^* < 0.9\}$: $5 \cdot 10^{-4} < (h/L)(H_I/L) < 2.5 \cdot 10^{-3}$, with $[0.0015 < D_{50,p}/L \leq 0.0035; 0.10 < B^*/L \leq 0.20]$.

The reflected energy and the energy dissipation rate are almost equal (or are in equilibrium) when $[K_R^2 \approx 0.5; D^* \approx 0.5]$. This state can exist whenever $(h/L)(H_I/L) \approx 4 \cdot 10^{-4}$, $D_{50,p}/L \approx 0.0015$, $B^*/L \approx 0.10$. The boundaries of these domains can change with the type of unit piece, the number of layers and configuration of the main armor layer, and definitively with the slope angle. Finally, the variability of the relative armor diameter and the number of layers is analyzed in Clavero et al. (2018).

5.2 Experimental deviation

The experimental deviation may come from two sources: (1) experimental scattering from the generation, analysis and separation methods used, and (2) experimental scattering from the physical processes. The wave generation and separation method is analyzed in the Supplementary Material provided with the paper. From the discussion and results shown in the Supplementary Material, we can assert that the experimental technique and method of analysis in themselves are not sufficient to explain the variability of the experimental values. The deviation is located in certain intervals of the value of I_r, as well as of $(h/L)(H_I/L)$.

5.2.1 Impermeable and non-overtoppable slope

Figure 8 represents the fit of a sigmoid curve to the experimental values of K_R^2 of the 1:2 impermeable slope against $I_{r,I}$ and $(h/L)(HI/L)$ (Fig. 8a.1 and 7a.2), as well as the residual values that fit a t-Student (Fig. 8b.1 and b.2). In (Fig. 8a.2), the experimental data alignment satisfactorily identifies the transitional domain, dissipative domain, and reflective domain: $[1.1 \cdot 10^{-3} < (h/L)(H_I/L) < 8 \cdot 10^{-3}]$,

$[(h/L)(H_I/L) \geq 10^{-2}]$, $[(h/L)(H_I/L) \leq 10^{-3}]$, respectively. The distribution of the residual values evidence that the deviation of the K_R^2 values, in absolute terms, is small in the dissipative domain in both representations. However, the scatter increases in the transitional domain and in the reflective domain in the Ir representation. The latter is also applicable to the dissipation rate D^* values.

Figure 8a.2 shows that if $(h/L)(H_I/L) < 2.8{\cdot}10^{-3}$, the reflection increases and the dissipation rate decreases, and that the breaker type evolves from a strong bore to strong plunging breaker. In contrast, if the product $(h/L)(H_I/L) > 2.8{\cdot}10^{-3}$, wave reflection decreases, dissipation increases, and the breaker type evolves from a strong plunging breaker to a strong bore and perhaps a weak bore.

Hence, in the domains in which either reflection or dissipation is dominant, the variability of the energy transformation mode and of the breaker type is delimited. Then, the values of K_R^2 and D^* do not change significantly with $(h/L)(H_I/L)$, contrary to what happens in the transitional zone. In the reflective domain, the type of wavebreaking remains practically constant. However, in the dissipative domain, if the slope and relative depth remain constant, the type of wave breaking also depends on wave steepness. In contrast, if h and L simultaneously increase, I_r also increases, and the breaker type evolves from a weak plunging to a strong plunging. If h and L simultaneously decrease, I_r also decreases and the breaker type evolves from a strong plunging to a weak plunging (Fig. 8a.2).

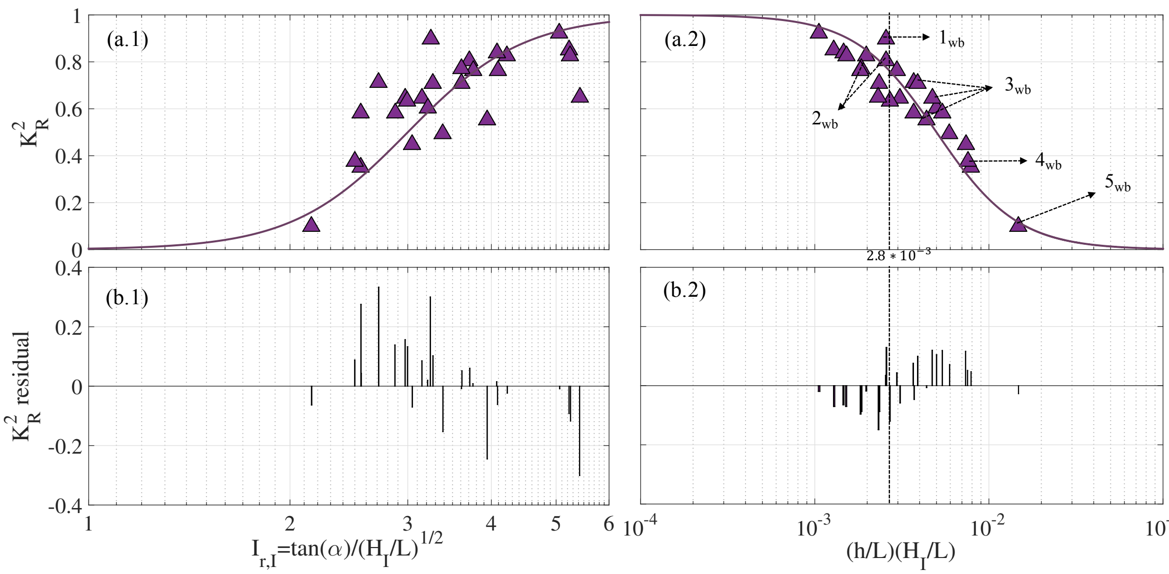

Figure 8. (a) Fit of the sigmoid curve to the experimental values of K_R^2 for the impermeable 1:2 slope against the experimental Iribarren number ($I_{r,I}$) and the product of relative depth and steepness (h/L)(HI/L). (b) Values of the deviation obtained from the residual values: experimental value less the theoretical value calculated by the sigmoid curve. The number j_{wb} (j=1:5) identifies the wave breaker types on the slope: 1_{wb} – surging, 2_{wb} – weak bore, 3_{wb} – strong bore, 4_{wb} – strong plunging, 5_{wb} – weak plunging.

5.2.2 Permeable with a main armor layer and non-overtoppable slope

If the breakwater is permeable, the relation between I_r and the energy transformation modes and breaker type deteriorates significantly since other processes come into play, namely the reflection and dissipation associated with the dimensionless variables ($D_{50,p}/L$, B^*/L, D_a/L, $n_l D_a/L$). Figure 9 represents the value pairs, ($I_{r,I}$, x_m/L), ($I_{r,I}$, B^*/L), which were tested in this research with a 1:2 slope angle. The results showed that a wide range of values of x_m/L and B^*/L corresponded to one value of $I_{r,I}$.

A comparison of these results to those of the impermeable breakwater with the same slope angle highlighted significant changes in the performance of the permeable breakwater (Fig. 10). The reflected energy decreased throughout the experimental interval, in other words, in all the modes of incident energy transformation and wavebreaking. The domains shifted towards lower values of $(h/L)(H_I/L)$, and the variation curves of K_R^2, K_T^2 and D^* depend on both $(h/L)(H_I/L)$ and B^*/L (and

$D_{50,p}/L$, D_a/L). Figure 10 shows the fit of a sigmoid curve to the experimental values of K_R^2 for the 1:2 permeable slope angle against $I_{r,I}$ and$(h/L)(HI/L)$ (Fig. 10a), as well as the residual values that fit a Student-*t* model (Fig. 10b). When the relative depth is incorporated on the *x*-axis (Fig. 10a.2), the alignment of the experimental data provides a reasonably good identification of the transitional domain [$5{\cdot}10^{-4} < (h/L)(H_I/L) < 3{\cdot}10^{-3}$], reflective domain [$(h/L)(H_I/L) \geq 3{\cdot}10^{-3}$], and dissipative domain [$(h/L)(H_I/L) \leq 4{\cdot}10^{-4}$]. Furthermore, it is visually evident, and confirmed by the residual distribution, that the deviation of the K_R^2 and D^* values is more pronounced in the transitional domain. The evolution of the modes of energy transformation and breaker type depends on the values of B^*/L (and $D_{50,p}/L$, D_a/L) with specific trajectories (see Fig. 7).

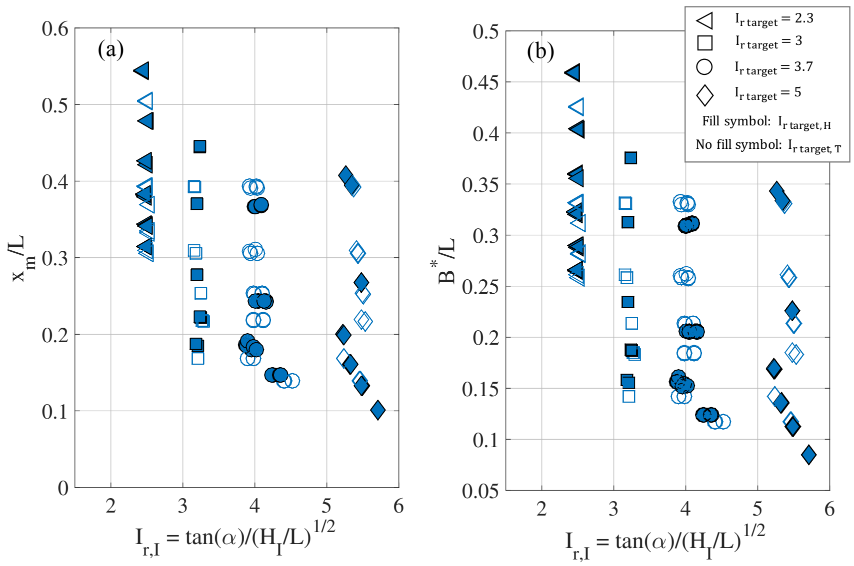

Figure 9. Experimental physical values (IISTA-UGR) of (a) x_m/L, (b) B^*/L, against the experimental Iribarren number ($I_{r,I}$), clustered according to the $I_{r\,target}$ tested in the laboratory.

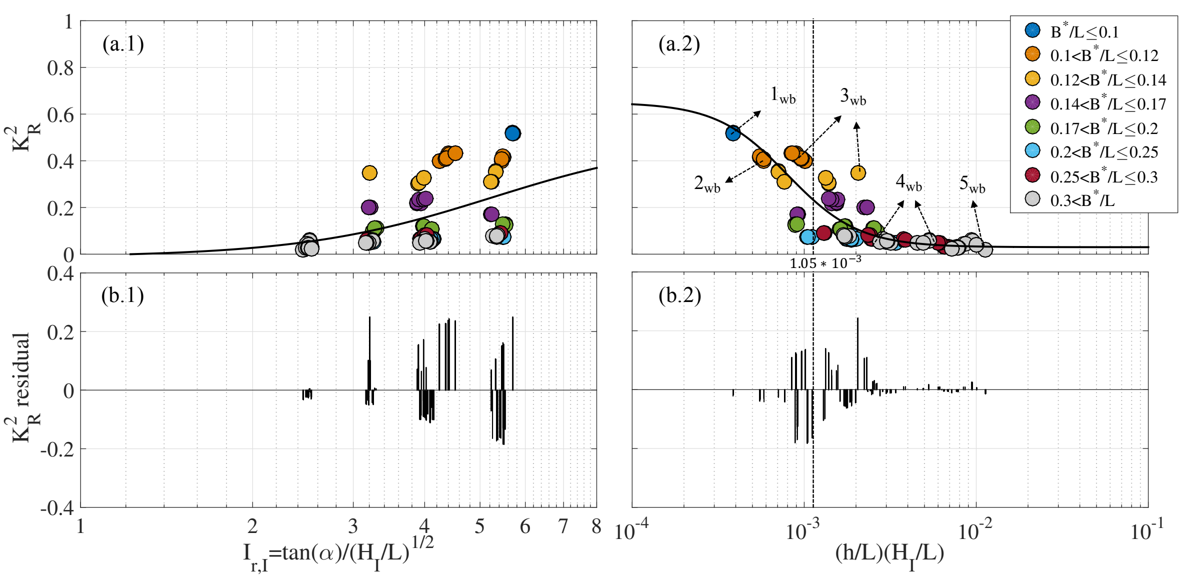

Figure 10. (a) Fit of the sigmoid curve to experimental values of K_R^2 for a 1:2 permeable slope angle, against the experimental Iribarren number ($I_{r,I}$) and the product of the relative depth and wave steepness $(h/L)(HI/L)$ according to intervals of values of B^*/L. (b) Values of the residual deviation: experimental value minus the theoretical value calculated with the sigmoid curve. The number j_{wb} (j=1:5) identifies the wave breaker types on the slope: 1_{wb} – surging, 2_{wb} – weak bore, 3_{wb} – strong bore, 4_{wb} – strong plunging, 5_{wb} – weak plunging.

The application of the modified Iribarren number, $I_r^* = (A_{eq}/L^2)/\sqrt{H_{trms}/L}$ (Clavero et al., 2018; Díaz-Carrasco et al., 2018) significantly corrects this behavior of the Iribarren number; being H_{trms} the total root-mean-square wave height at the toe of the breakwater. The domains can thus be identified since the deviation decreases in the transitional domain and the reflective domain, whereas it increases in the dissipative domain. In other words, I_r^* improves prediction when the transformation processes in the core, particularly in the case of reflection, dominate those on the slope. Nevertheless, this representation does not permit the identification of the possible breaker types in each domain.

5.3 Wave transformation similarity and the log-transformation of the experimental space

In a real breakwater located in intermediate/shallow waters (e.g., h = 10 m, T = 10 s, H = 5 m, 5 < B^* (m) < 10 and 0.10 < $D_{50,p}$ (m) < 0.25), $R_{e,p} > 10^5$, fully turbulent regime), it is improbable that all of the regime changes observed in the laboratory will occur. For the values of [K_R^2, K_T^2, D^*] obtained in a model to be representative of the prototype values, besides complying with the Froude scale, the dissipation-reflection-transmission processes of the wave train in the core should be similar to those of the prototype. One way to verify this condition is to select the two dimensionless quantities, B^*/L, $D_{50,p}/L$ in order to satisfy the model-prototype equivalent hypothesis of Lorentz (Pérez-Romero et al., 2009; Vílchez et al., 2016) in each run of H and T.

Figure 11a represents the space [ln(h/L), ln(H_I/L), B^*/L (or $D_{50,p}/L$)] of the experimental values obtained in the laboratory. Figure 11b represents the space [ln(h/L), ln(H_I/L] of the experimental values with slope angle 1:2 obtained in the numerical model. The tendency and the wavebreaking bands are identified, as well the isolines of the constant product (h/L)(H_I/L). It is observed that there is not a biunivocal relationship between I_r and the type of breaker. Figure 11 facilitates the creation of a suitable experimental design in the laboratory, since it includes the information needed to fulfill the prototype-model equivalent hypothesis of Lorentz (B^*/L, $D_{50,p}/L$). Additonally, Figure 11 identifies combinations of H and T that delimit the three intervals of the energy transformation modes for any mound breakwater typology.

6. Conclusions

The main objective of this research is to characterize and quantify the prevalent physical processes in the energy transformation of a regular wave train while interacting with permeable or impermeable breakwaters. Two sources of experimental data are considered: (a) numerical experiments on an undefined impermeable rigid slope with the numerical model (IH-2VOF), and (b) physical experiments on a non-overtoppable permeable breakwater with a cube armor layer and a porous core of finite width in a 2D wave flume. Simultaneously, the dependence of wave energy transformation processes (reflection, transmission, and dissipation) with Iribarren number is collated and its role as surf similarity parameter is discussed. The following conclusions can be derived from this study:

(1) Applying dimensional analysis to the wave interaction with non-overtoppable, impermeable slopes, the relationship between the reflected energy coefficient, K_R^2, and the product of the relative water depth, h/L, and wave steepness at the toe of the slope, H_I/L, is deduced. The wave energy conservation equation enables to extent this result to the wave dissipation, $D*$. The slope angle is a parameter of the problem since it cannot be expressed in terms of the dimensional base.

(2) Similarly, in the case of permeable slopes with a main armor layer and a porous core, in addition to (h/L)(H_I/L), the reflection and transmitted coefficients, [K_R^2, K_T^2], depend on $D_{50,p}/L$, B^*/L, D_a/L, n_lD_a/L. Again, the slope angle is a parameter, and the wave energy conservation equation enables the calculation of the bulk wave dissipation, D^*.

(3) Plotting [K_R^2, K_T^2, D^*] against (h/L)(H_I/L) three wave energy transformation domains are easily defined: dissipative, transitional and reflective. In each of them a set of most probable breaker types can be identified.

(4) In the transitional domain, different combinations of wave energy transformation mode and breaker type can occur with a constant Iribarren number: there is not a biunivocal relationship between I_r and (i) the type of breaker, (ii) the reflection and transmission coefficients and (iii)

the bulk dissipation. Therefore, at least in the transitional domain, Iribarren´s number is not a sufficient similarity parameter for the analysis of wave breaking, and related flow characteristics on slopes.

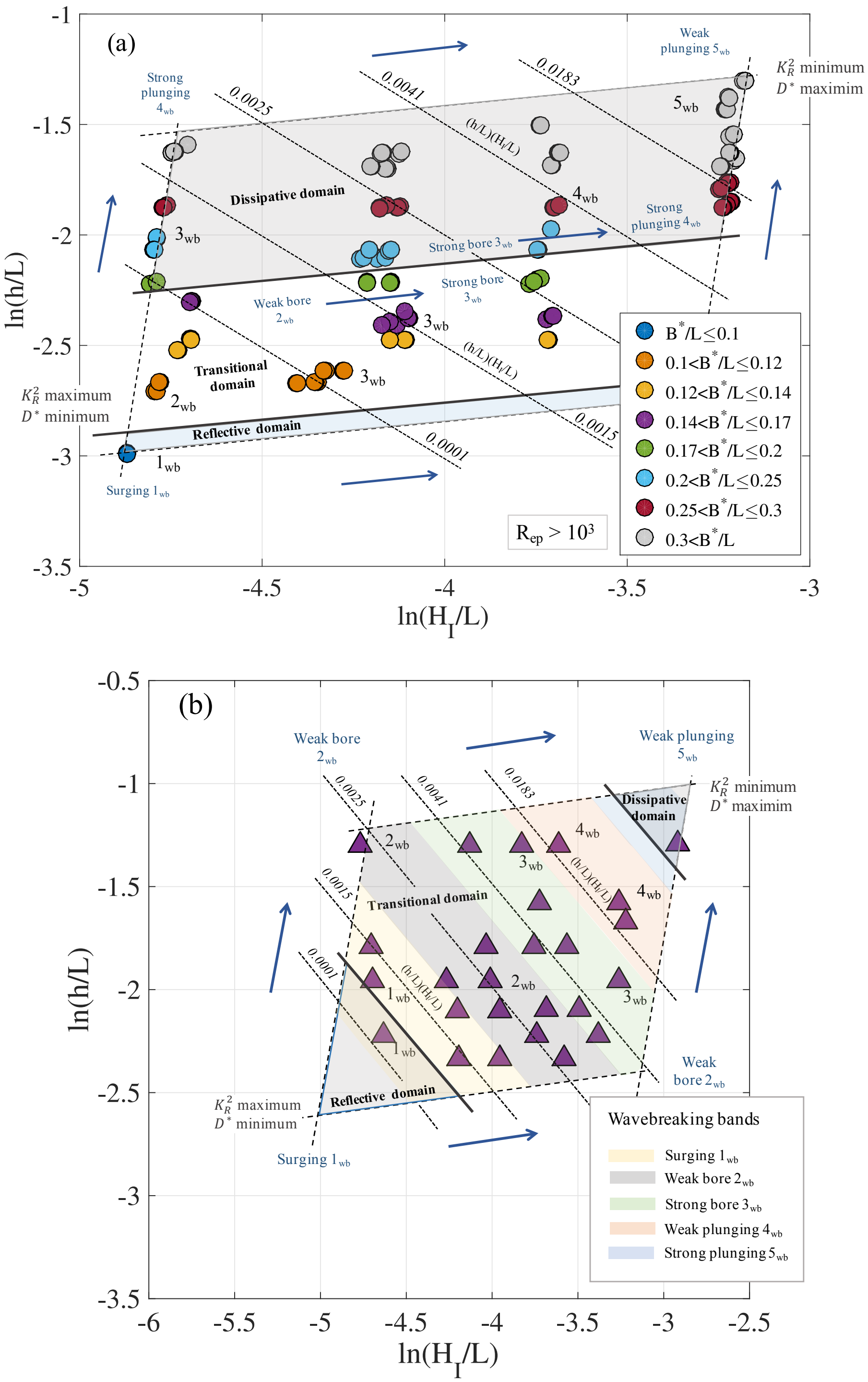

Figure 11: Experimental space [ln(h/L), ln(H_I/L)] of (a) the laboratory tests with a slope angle 1:2 according to ranges of values of the monomial B^*/L (colors); (b) the numerical tests with a slope angle 1:2 and wavebreaking bands represented by colors. In both figures the tendency of the wavebreaking is marked with solid blue arrows and the following domains were also identified: (1) reflective domain; (2) dissipative domain; and (3) transitional domain.

(5) A sigmoid function of the variable $(h/L)(H_I/L)$ fits reasonable well the experimental results $[K_R^2, K_T^2, D^*]$, for impermeable as well as for permeable slopes. A poor fit is obtained when the Iribarren number taken the independent variable. These conclusions are confirmed by the representation of the residual error between the experimental data and the fitted curve.

(6) Because the range of the design factors spans several orders of magnitude, the log-transformation of the experimental space $[\ln(h/L), \ln(H/L)]$ is likely benefit to elaborate a suitable experimental design in laboratory, which allows verifying the wave breaker type and the related dissipation-reflection-transmission on slopes.

Acknowledgements

This work was supported by the research group TEP-209 (Junta de Andalucía) and by two projects: (1) "Protection of coastal urban fronts against global warming – PROTOCOL" (917PTE0538) and (2) "Integrated verification of the hydrodynamic and structural behavior of a breakwater and its implications on the investment project – VIVALDI" (BIA2015-65598-P). The work of the first author was funded by the Spanish Ministry of Education, Culture and Sports (Research Contract FPU14/03570). The second author was funded by the "Garantía Juvenil" program (Social European Grant).

Appendix A. Wave-mound breakwater interaction: dimensional analysis

A.1 Problem definition

Dimensional analysis involves four stages: (1) identification of a complete set of *n* independent quantities; (2) selection of a complete subset of *k* dimensionally independent quantities; (3) definition of (*n-k*) independent quantities, based on the power products of the *k* quantities selected; (4) application of the $\prod$ theorem to express dependent quantities as a function of the (*n-k*) independent quantities.

Impermeable and non-overtoppable slope

The complete set of independent variables that participate in the transformation of the wave train on an impermeable slope consists of the following: (i) slope angle, α; (ii) water depth, h; (iii) incident wave height, H_I; (iv) wave period, T_Z, (or wave length, L); (v) gravity acceleration, g,; (vi) dynamic viscosity, μ; and water density, ρ. The effect of the surface tension and water compressibility is negligible. Excluding α,

$$X = f(h, \rho, \mu, g, H_I, L)$$
$$X = (X_1, X_2) = (H_R, X_{0,R})$$

where X denotes the set of dependent variables, the wave height and the phase of the reflected wave train. $X_{0,R}$ is the distance measured from the toe of the slope to the location of the point reflector of the reflected wave train.

Accordingly, $\{\rho, g, L\}$ are selected as the complete subset of the dimensionally independent quantities (k=3). The remaining variables of the set and the dependent quantities (i.e. characteristics of the reflected wave train) can be expressed as power products of this dimensional base, $(n\text{-}k) = 3$, to obtain the similarity equation

$$X^* = [H_R/L, X_{0,R}/L] = f_1(h/L, H_I/L, R_{e,w})$$

When the kinematic viscosity is represented by $\nu = \mu/\rho$, the third dimensionless variable, $R_{e,w} \approx U_c h/\nu$, is a Reynolds number, whose value should be sufficiently high for the regime to be regarded as fully developed turbulence. U_c is a characteristic velocity, in general the maximum, of the oscillatory movement in the water column (Keulegan and Carpenter, 1958).

The slope angle, α, is not included since it is a dimensionless quantity, and thus can not be expressed in terms of the base. Since dimensional analysis cannot provide information about the way that wave transformation depends on the slope angle, n-k = 3. For the same reason, it is not possible to include ϕ_R and consider the distance $X_{0,R}$, is considered, which like H_R is a quantity of the first kind.

Sutherland and O´Donoghue (1998) experimentally verified that the reflection phase ϕ_R depends on h/L and the slope angle. They proposed that it should be related to the dimensionless variable x_m/L, where x_m is the horizontal distance of the slope from the toe to the cut with the surface of the sea at rest. Thus, alternatively, x_m/L can be included in the complete set of independent variables, then n = 7 and (n-k) = 4,

$X = \mathrm{f}(h, x_m, \rho, \mu, g, H_I, L)$

$X^* = [H_R/L, X_{0,R}/L] = \mathrm{f}_1(h/L, x_m/L, H_I/L, R_{e,w})$

In this work, for clarity of exposition, the slope angle has been chosen to use as an "identificative parameter" of the results, instead of incorporating x_m/L in the function. Recall that, by definition $x_m/L = (1/\tan(\alpha))(h/L)$.

The total energy of the incident and reflected wave trains are derived quantities that are expressed as follows:

$E_I/(\rho g L) = (1/8)H_I^2$; $E_R/(\rho g L) = (1/8)H_R^2$

$K_R^2 = H_R^2/H_I^2 = E_R/E_I$; $\phi_R \propto X_{0,R}/L$

Finally, the dependent quantity (reflected energy coefficient and phase of the reflected wave train) are:

$$[K_R^2, \frac{X_{0R}}{L}] = \Psi_R(h/L, H_I/L) \tag{3}$$

Although the function Ψ is undetermined, its form is similar for all possible slope angles. Finally, the dissipation rate for the mean incident energy flow, which is a dimensionless variable of the second kind, is calculated as follows (Eq. 1),

$$D^* = 1 - \Psi_R(h/L, H_I/L) \tag{4}$$

Permeable with a main armor layer and non-overtoppable slope

The difference in performance in this permeable breakwater and in the impermeable slope stems from the additional dissipative regimes: (1) in the main armor layer, and (2) during wave propagation in the porous medium (see Section 2). Hence, for this permeable breakwater, the complete set of independent variables participating in the transformation of the wave train, is considerably larger than in the case of an impermeable slope. Again, excluding α and β, the seaward and landward slope angles, respectively

$(X_1, X_2) = \mathrm{f}(h, \rho, \mu, g, H_I, L, D_{50,p}, B^*, D_a, e)$

Where B^* is a characteristic width of the granular core of uniform size, $D_{50,p}$; D_a is the equivalent diameter of the type and shape of the unit piece of the main armor layer, positioned with a specific placement criterion; e represents its thickness, which can be expressed in terms of the equivalent diameter of the unit piece ($e = n_l D_a$), where n_l is a real number; (X_1, X_2) are the two dependent variables, which in this case are the statistical or spectral descriptors of the wave height and reflected wave train, [H_R or $(m_{0,R})^{1/2}$, $X_{0,R}$], and of the transmitted wave train, [H_T or $(m_{0,T})^{1/2}$, $X_{0,T}$], respectively. Generally, $X_{0,T}$, is the distance measured from the toe of leeward slope to the location of the point transmitter of the transmitted wave train. Alternatively, it had be possible to include $x_{m,s}$ and $x_{m,l}$, seaward and landward horizontal length of the slope, respectively.

In the same way as for the impermeable slope, $\{\rho, g, L\}$ are selected as the complete subset of dimensionally independent quantities ($k=3$). The remaining variables of the set and the dependent variable, can be expressed as the power product of this dimensional base, (n-k) = 7, (similarity equation),

$$X_1^* = [H_R/L, X_{0,R}/L] = \mathrm{f}_1(h/L, H_I/L, D_{50,p}/L, B^*/L, D_a/L, R_{eDa}, R_{e,p})$$

$$X_2^* = [H_T/L, X_{0,T}/L] = \mathrm{f}_2(h/L, H_I/L, D_{50,p}/L, B^*/L, D_a/L, R_{eDa}, R_{e,p})$$

The similarity equations incorporate four new dimensionless variables: D_a/L, and $R_{e,Da}$ the relative armor diameter and an armor Reynolds number. They respectively govern the turbulence regime on the slope due to the breaking and interaction of the wave train with the main armor layer, mainly dissipation (Clavero et al., 2018). Like the forces inside the core, the force regimes in the armor layer are determined in function of $R_{e,Da}$ and $R_{e,Da}/KC_a$, where $KC_a \approx H_I/D_a$ is the armor Keulegan-Carpenter number. $R_{e,Da}$ is a reformulation of $R_{e,w}$, and was identified in the case of the impermeable slope. The grain Reynolds number, $R_{e,p}$ characterizes the hydrodynamic regime inside the core (Burcharth and Andersen, 1995). The dimensionless quantities $D_{50,p}/L$ and $A_{eq}/L^2 \approx (h/L)\,(B^*/L)$ govern the dissipation of the flow (Pérez-Romero et al., 2009), and the reflection and phase inside the porous core (Vílchez et al., 2016a), respectively.

The total energy of the incident, reflected, and transmitted wave trains are derived dimensionless quantities of the first kind, which are expressed as follows:

$$\mathrm{E_I}/(\rho g L) = (1/8)H_I^2;\;\; \mathrm{E_R}/(\rho g L) = (1/8)H_R^2;\;\; \mathrm{E_T}/(\rho g L) = (1/8)H_T^2$$

$$K_T^2 = H_T^2/H_I^2 = \mathrm{E_T}/\mathrm{E_I};\;\; \phi_T \propto X_{0,T}/L$$

Finally, the dependent quantity (reflected and transmitted energy coefficient and phase of the reflected and transmitted wave train) are,

$$[\mathrm{K_R}^2, \frac{X_{0R}}{L}] = \Psi_\mathrm{R}(\mathrm{h/L, H_I/L, D_{50,p}/L, B^*/L, D_a/L, R_{eDa}, R_{e,p}}) \quad (5)$$

$$[\mathrm{K_T}^2, \frac{X_{0T}}{L}] = \Psi_\mathrm{T}(\mathrm{h/L, H_I/L, D_{50,p}/L, B^*/L, D_a/L, R_{eDa}, R_{e,p}}) \quad (6)$$

where, despite the fact that functions (Ψ_R,Ψ_T) are undetermined, their form is similar for the value pairs of the leeward and landward slope angles considered. Moreover, in order to apply the results to the scale of the prototype, the Reynolds number values of the layer, R_{eDa}, and grain $R_{e,p}$, should be sufficiently high so that the hydrodynamic regime of each run is totally turbulent in the water column, and inside the main layer and the core.

Bulk dissipation includes the shoaling-associated dissipation, interaction with the main armor layer and the evolution of the wave profile, which would include eventual wave breaking, and the dissipation during the propagation and transmission of the wave train through the porous core. This bulk dissipation ($D^{'*}$), a dimensionless quantity of the second kind, is determined on the basis of experimental results, solving the conservation energy equation:

$$\mathrm{D}^* = \mathrm{D}^{'*}/(\mathrm{C_g\, E_I}) = 1 - \Psi_\mathrm{R} - \Psi_\mathrm{T} \quad (7)$$

Finally, it should be highlighted that even though the $R_{e,w}$ R_{eDa}, and $R_{e,p}$ values exceed the threshold, this does not signify a reduction in the number of independent variables in the initial set. The similarity equation cannot be simplified, and since the dependence of the Reynolds numbers is implicit in the experimental results, and it cannot be ignored.

A.2 Experimental design based on dimensional analysis

The response of the dependent dimensionless quantities, $[K_R^2, \frac{X_{0R}}{L}, \mathrm{K_T}^2, \frac{X_{0T}}{L}]$ (first kind) are functions of the set of input/predictor dimensionless quantities, (Eq. 3, 5 and 6). In the case of the impermeable slope, Ψ: $\Re^2 \rightarrow \Re^3$, whereas for the sloping breakwater with a porous core and a main armor layer, Ψ: $\Re^2 \rightarrow \Re^5$ (where $\Re^n$ is the real space of n non-dimensional quantities). In all cases, wave generation were chosen based on two dimensionless quantities that characterize the incident wave train at the toe of the slope breakwater: the wave steepness, (H_I/L), and relative depth, (h/L).

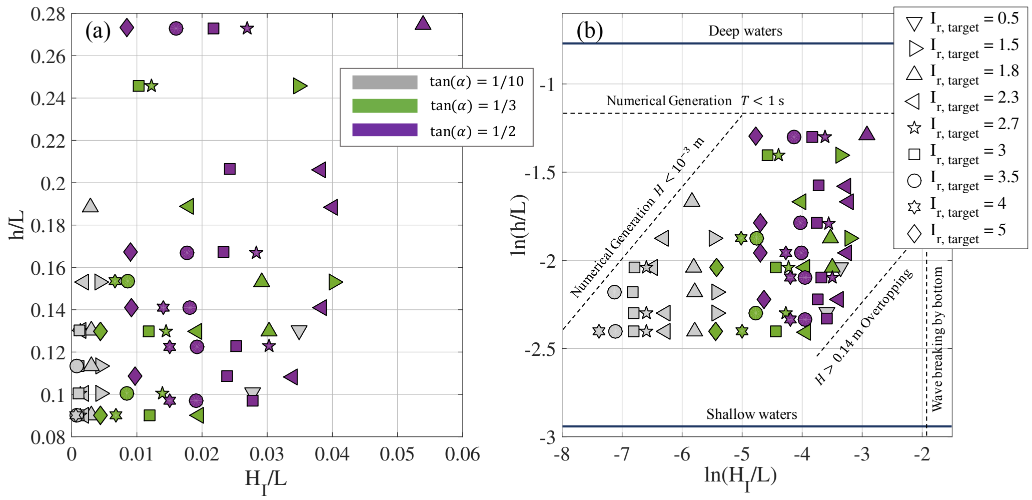

Figure 12: Experimental value of the impermeable slope for each $I_{r\ target}$ (symbols) and three slope angles (colors) numerically simulated in: (a) space [h/L, H_I/L]; (b) log-transformation space [ln(h/L), ln(H_I/L)]. Figure 12b shows the experimental limits for wave generation in the numerical model, wave breaking due to the water depth, and the non-overtopping condition.

Figure 12 represents the pairs of experimental values of the impermeable breakwater in space [h/L, H_I/L] (Fig. 13a), and in the space [ln(h/L), ln(H_I/L)] (Fig. 12b), after log-transformation. The corresponding values of the permeable porous breakwater are shown in Figure 13a. Figure 13b identifies two dimensionless quantities for this type of breakwater, [ln(B^*/L), ln($D_{50,p}/L$)]. Though not shown in Figure 13, the breakwater slope is 1:2, a double layer of cube armor of diameter D_a = 0.0409 m. After the log-transformation, the dimensionless quantities may become more independent (fewer interactions), and facilitate (1) the selection of highly representative experimental results, (2) the optimization of the number of experiments and (3) the minimum number of repetitions in order to satisfactorily combine multivariate dimensional analysis with statistical analysis (Albrecht et al., 2013).

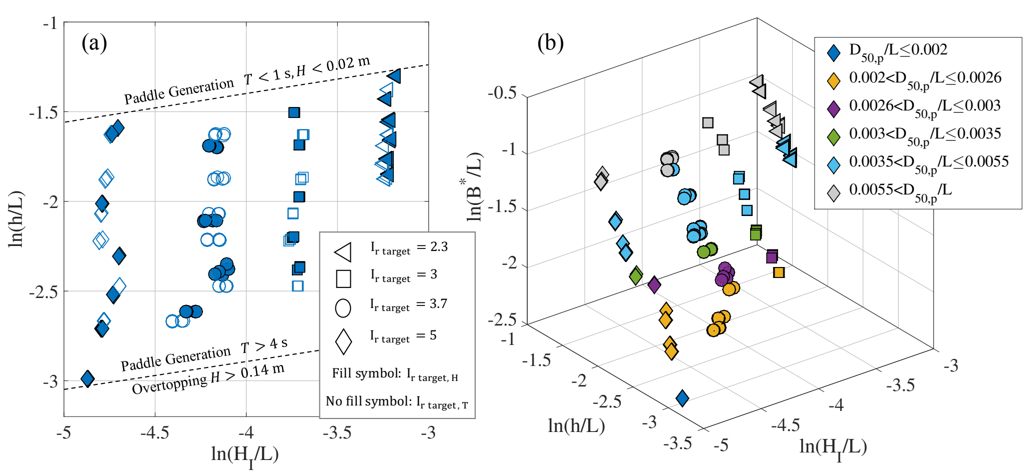

Figure 13. Experimental values of the permeable slope with a main layer and porous core: (a) space [ln(h/L), ln(H_I/L)] for each $I_{r\ target}$ tested; (b) log-transformed space [ln(B^*/L), ln(h/L), ln(H_I/L)], which uses different colors to show the value ranges of the monomial $D_{50,p}/L$.

List of symbols

A_{eq}	Equivalent area of the porous medium below the water level
B^*	Characterized width of the breakwater
B_b	Width of the top of the breakwater
C_g	Group celerity
$C_{g,target}$	Target value of the group celerity
C_{target}	Target value of the celerity
$D^{`*}$	Mean bulk dissipation
D^*	Wave energy dissipation rate
$D_{50,p}$	Grain size
D_a	Characteristic diameter of the main armor layer
D_{eq}	Equivalent diameter of the main armor layer
e	Equivalent diameter
E_I	Incident wave energy
E_R	Reflected wave energy
E_T	Transmitted wave energy
E_{target}	Target value of the wave energy
F_I	Mean energy flow of the incident wave train
f_I	Inertial force
f_L	Laminar force
F_{MT}	Porous medium height
F_R	Mean energy flow of the reflected wave train
F_T	Mena energy flow of the transmitted wave train
f_T	Turbulent force
g	Gravity acceleration
h	Water depth
H	Wave height
H_I	Incident wave height
H_R	Reflected wave height
H_T	Transmitted wave height
H_{trms}	Total root-mean-square wave height
H_{target}	Target value of wave height
I_r	Iribarren number
$I_{r,\ target}$	Target value of iribarren number
j_{wb}	J=[1-6] identifies the breaker types
KC_p	Keulegan-Carpenter number
K_R	Modulus of the reflection coefficient
K_T	Modulus of the transmission coefficient
L	Wave length
L_{target}	Target value of wave length
m_0	Zero-order momentum
n_l	Real number
n_p	Core porosity
$R_{e,w}$	Reynolds number
R_{eDa}	Armor reynolds number
Re_p	Granular reynolds number
T	Wave period
T_{target}	Target value of wave period
T_Z	Mean wave period
$T_{z,target}$	Target value of the mean wave period
U_c	Characteristic velocity of the water column
U_p	Characteristic seepage velocity
$X_{0,R}$	Reflection dimensional phase
$X_{0,T}$	Transmission dimensional phase
x_m	X_m=h/tan(α) intersection of the mwl with the seaward slope of the breakwater

α Seawards slope angle
β Leeward slope angle
μ Dynamic viscosity
ρ Water density
ρ_s Unit piece density
Ψ Represent the functional relationship
θ Incidence angle
ν Kinematic viscosity
ϕ_R Reflection phase

References

Albrecht, M.C., Nachtsheim, C.J., Albrecht, T., Cook, R.D., 2013. Experimental Design for Engineering Dimensional Analysis. Technometrics, 55 (3).

Allsop, N.W.H., Channell, A.R., 1989. Wave reflections in harbours: reflection performance of rock armoured slopes in random waves. Technical Report OD 102. Hydraulics Research, Wallingford.

Baquerizo, A., 1995. Reflexión del oleaje en playas. Métodos de evaluación y de predicción (PhD thesis), University of Cantabria (in Spanish).

Battjes, J.A., 1974. Surf Similarity. Proc. 14th International Conference of Coastal Engineering. ASCE, pp. 466-480.

Benedicto, M.I., 2004. Comportamiento y evolución de la avería de los diques de abrigo frente a la acción del oleaje (PhD thesis), University of Granada (in Spanish).

Burcharth, H.F., Andersen, O.K., 1995. On the one-dimensional steady and unsteady porous flow equations. Coastal Engineering. 24 (3–4), 233–257.

Burcharth, H.F., Andersen, T.L., Medina, J.R., 2010. Stability of Cubipod Armoured Roundheads in Short Crested Waves. Proc. 32nd International Conference of Coastal Engineering. ASCE.

Bruun, P. and Günbak, A.R., 1976. New design principles for rubble mound structures. Proc. 15th International Conference of Coastal Engineering Conference. ASCE, pp. 2429-2473.

Christensen, E.D., Deigaard, R., 2001. Large eddy simulation of breaking waves. Coastal Engineering, 42, 53-86.

Churchill, S.W., Usagi, R., 1972. A general expression for the correlation of rates of transfer and other phenomena. AICHE J. 18, 11221–1128.

Clavero, M., Folgueras, P., Díaz-Carrasco, P., Ortega-Sánchez, M., Losada, M.A., 2018. A similarity parameter for breakwaters: the modified Iribarren number. Proc. 36th International Conference of Coastal Engineering. ASCE, Baltimore (Maryland, USA).

CIRIA, CUR, CETMEF, 2007. The Rock Manual: The Use of Rock in Hydraulic Engineering. CIRIA, London, p. C683.

Cyril, J., Galvin, J.R., 1968. Break type classification on the three laboratory beaches. Journal of Geophysical Research, 73, 3651-3659.

Dai, Y.B., Kamel, A.M., 1969. Scale effect tests for rubble-mound breakwaters: Hydraulic Model Investigation. U.S. Army Engineer Waterways Experiment Station. Hydraulic Engineering Reports.

Dalrymple, R.A., Losada, M.A., Martín, P.A., 1991. Reflection and transmission from porous structures under oblique wave attack. Journal of Fluid Mechanics, 224, 625–644.

Davidson M.A., Bird P.A.D., Bullock G.N., Huntley D.A, 1996. A new non-dimensional number for the analysis of wave reflection from rubble mound Breakwaters. Coastal Engineering, 28, 93-120

Díaz-Carrasco, P., Moragues, M.V., Clavero, M., Ortega-Sánchez, M., Losada, M.A, 2018. Similarity on Rubble-Mound Breakwaters tests: analysis and discussion. Proc. 7th International Conference on the Application of Physical Modelling in Coastal and Port Engineering and Science, Santander, Spain.

Díaz-Carrasco, P., Røge, M.S., Andersen, T.L., 2019. Wave-Breakwater interaction: Test Program in the Flume of Aalborg University. Technical documentation, Department of Civil Engineering, Aalborg University.

Frigaard, P., Andersen, T. L., 2014. Analysis of Waves: Technical documentation for WaveLab 3. Aalborg: Department of Civil Engineering, Aalborg University. DCE Lecture notes, No. 33.

Gíslason, K., Fredsoe, J., Deigaard, R., Sumer, B.M., 2009. Flow under standing waves: Part 1. Shear stress distribution, energy flux and steady streaming. Coastal Engineering, 56, 341-362.

Gómez-Martín, M.E., Medina, J.R., 2014. Heterogeneous Packing and Hydraulic Stability of Cube and Cubipod Armour Units. Journal of Waterway, Port, Coastal and Ocean Engineering, 140, 100-108.

Gu, Z., Wang, H., 1991. Gravity waves over porous bottom. Coast. Eng. 15, 497–524.

Hughes, S.A., Fowler, J.E., 1995. Estimating wave-induced kinematics at sloping structures. Journal of. Waterway Port Coastal and Ocean Engineering. 209–215.

Iribarren, R., Nogales, C., 1949. Protection des Ports. XVII International Navigation Congress, Lisbon (1949).

Iversen, H.W., 1952. Laboratory study of breakers. Natl. Bur. Standards, Circular 521, 9-32. “Gravity Waves”, Washington, D.C.

Jensen, B., Christensen, E.D., Sumer, B.M., 2014a. Pressure-induced forces and shear stresses on rubble mound breakwater armour layers in regular waves. Coastal Engineering, 91, 60-75.

Jensen, B, Jacobsen, N.D., Christensen, E.D., 2014b. Investigations on the porous media equations and resistance coefficients for coastal structures. Coastal engineering, 84, 56-72.

Keulegan, G. H.; Carpenter, L. H., 1958. Forces on cylinders and plates in an oscillating fluid". Journal of Research of the National Bureau of Standards, 60, 423–440.

Kobayashi, N., Wurjanto, A., 1992. Irregular Wave Interaction with Permeable Slopes. Proc. 23^{rd} International Conference of Coastal Engineering. ASCE, 118, pp. 368-386.

Kortenhaus, A., Oumeraci, H., 1998. Classification of wave loading on monolithic coastal structures. Coastal Engineering, 867–880.

Lakehal, D., Liovic, P., 2011. Turbulence structure and interaction with steep breaking waves. Journal of Fluid Mechanics, 674, 522-577.

Lara, J.L., Losada, I.J., Liu, P.L-F. 2006. Breaking waves over a mild gravel slope: Experimental and numerical analysis. Journal of Geophysical Research Atmospheres, 111 C11019.

Lara, J.L., Losada, I.J., Guanche, R., 2008. Wave interaction with low-mound breakwaters using a RANS model. Ocean Engineering, 35, 1388–1400.

Losada, M.A., Gimenez-Curto, L.A., 1981. Flow characteristics on rough, permeable slopes under wave action. Coastal Engineering, 4, 187–206.

Losada, I.J., Losada, M.A., Baquerizo, A., 1993. An analytical method to evaluate the efficiency of porous screens as wave dampers. Applied Ocean Research, 15, 207–215.

Losada, M.A., Díaz-Carrasco, P., Moragues, M.V., Clavero, M., 2019. Variabilidad intrínseca en el comportamiento de los diques rompeolas. XV Jornadas Españolas de Costas y Puertos. Torremolinos, Málaga (Spain) (in Spanish).

Madsen, P.A., Fuhrman, D.R., 2008. Run-up of tsunamis and long waves in terms of surf-similarity. Coastal Engineering, 55, 209-223.

Mansard, E.P.D., Funke, E.R., 1987. On the reflection analysis of irregular waves. Natl. Res. Cunc. Rev. Can. Hydraulics Laboratory Technical Report, TR-HY-O17.

Martin, F.L., Losada, M.A., Medina, R., 1999. Wave loads on rubble mound breakwater crown walls. Coastal Engineering, 37, 149–174.

Méndez, F.J., Losada, I.J., Dalrymple, R.A., Losada, M.A., 1998. Effects of wave reflection and dissipation on wave-induced second order magnitudes. Proc. 26^{th} International Conference of Coastal Engineering, pp. 537-550.

Moraes, C.C., 1970. Experiments of Wave Reflexion on Impermeable slopes, Proc. 12^{th} International Conference of Coastal Engineering, Washington, D.C., 1, pp. 509-521.

Pérez-Romero, D.M., Ortega-Sánchez, M., Moñino, A., Losada, M.A., 2009. Characteristic friction coefficient and scale effects in oscillatory porous flow. Coastal Engineering, 56, 931–939.

Requejo, S., Vidal, C., Losada, J.I., 2002. Modelling of waves loads and hydraulics performance of vertical permeable structures. Coastal Engineerging, 46, 249-276.

ROM, 0.0, 2001. Description and Characterization of Project Factors of Maritime Structures - 0.0. Retrieved from http://www.puertos.es/es-es/BibliotecaV2/ROM%200.0-01%20(EN).pdf.

ROM, 1.1, 2018. Recommendations for Breakwater Construction Projects - 1.1 Articles. Retrieved from http://www.puertos.es/es-es/ROM/Paginas/ROM-widispe.aspx (in Spanish).

Ruju, A., Lara, J.L., Losada, I.J., 2014. Numerical analysis of run-up oscillations under dissipative conditions, Coastal Engineering, 86, 45–56.

Seelig, W.N., J.P. Ahrens, 1981. Estimation of wave reflection and energy dissipation coefficients for beaches, revetments and breakwaters. CERC Technical paper 81-1, Fort Belvoir, U.S.A.C.E., Vicksburg, MS.

Sivanesapillai, R., Steeb, H., Hartmaier, A., 2014. Transition of effective hydraulic properties from low to high Reynolds number flow in porous media. Geophysical Research Letter, 41.

Sollitt, C.K., Cross, R.H., 1972. Wave transmission through permeable breakwaters. Proc., 13^{th} International Conference on Coastal Engineering. ASCE, Vancouver, pp. 1827–1846.

Sutherland, J., O'Donoghue, T., 1998. Wave phase shift at coastal structures. Journal of Waterway, Port, Coastal, and Ocean Engineering, 124, 534–550.

Ting, F.C.K., Kirby, J.T., 1996. Dynamics of surf-zone turbulence in a spilling breaker. Coastal Engineering 27, 131–160.

Van der Meer, J. W. ,1988. Rock slopes and gravel beaches under wave attack. (Phd Thesis) Delft Hydraulics.

Van der Meer, J.W., 1992. Conceptual design of rubble mound breakwaters. Proc. of a short course on the design and reliability of coastal structures, attached to 23rd Conference of Coastal Engineering, Venice. Tecnoprint, 447-510.

Van Der Meer, J., 2011. Design aspects of breakwaters and sea defences. In: 5th International Short Conference on Applied Coastal Research, Aachen (Germany).

Van Gent, M.R., 1995. Wave Interaction with Permeable Coastal Structures. (Phd Thesis) Delft University.

Van Gent, M.R., 2013. Rock stability of rubble mound breakwaters with a berm. Coastal Engineering, 78, 35–45.

Vanneste, D., Troch, P., 2015. 2D numerical simulation of large-scale physical model tests of wave interaction with a rubble-mound breakwater, Coastal Engineering ,103, 22–41

Vílchez, M., Clavero, M., Losada, M.A., 2016a. Hydraulic performance of different non-overtopped breakwater types under 2D wave attack. Coastal Engineering, 107, 34-52.

Vílchez, M., Clavero, M., Lara, J. L., and Losada, M. A., 2016b. A characteristic friction diagram for the numerical quantification of the hydraulic performance of different breakwater types. Coastal Engineering, 114, 86-98.

Wellens, P., Van Gent, M., 2012. Wave-induced setup inside permeable structures. Proc. 33rd International Conference of Coastal Engineering, 43.

Zanuttigh, B., van der Meer, J.W., 2008. Wave reflection from coastal structures in design conditions. Coastal Engineering, 55, 771–779.

Zhang, Q., Liu, P.L.F., 2006. A numerical study of bore runup a slope. Advance in Engineering Mechanics – Reflection and Outlooks.

Zhang, Q., Liu, P.L. F., 2008. A numerical study of swash flows generated by bores. Coastal Engineering, 55,1113-1134.